Predicting the Three-Dimensional Structure of the Human Facilitative Glucose Transporter Glut1 by a Novel Evolutionary Homology Strategy: Insights on the Molecular Mechanism of Substrate Migration, and Binding Sites for Glucose and Inhibitory Molecules

Alexis Salas-Burgos,* Pavel Iserovich,* Felipe Zuniga,† Juan Carlos Vera,† and Jorge Fischbarg*‡

*Department of Ophthalmology, College of Physicians & Surgeons, Columbia University, New York, New York; †Department of Pathophysiology, School of Sciences, University of Concepción, Chile; and ‡Department of Physiology and Biophysics, College of Physicians & Surgeons, Columbia University, New York, New York

ABSTRACT The glucose transporters (GLUT/SLC2A) are members of the major facilitator superfamily. Here, we generated a three-dimensional model for Glut1 using a two-step strategy: 1), GlpT structure as an initial homology template and 2), evolutionary homology using glucose-6-phosphate translocase as a template. The resulting structure (PDB No. 1SUK) exhibits a water-filled passageway communicating the extracellular and intracellular domains, with a funnel-like exofacial vestibule (infundibulum), followed by a 15 Å-long × 8 Å-wide channel, and a horn-shaped endofacial vestibule. Most residues which, by mutagenesis, are crucial for transport delimit the channel, and putative sugar recognition motifs (QLS, QLG) border both ends of the channel. On the outside of the structure there are two positively charged cavities (one exofacial, one endofacial) delimited by ATP-binding Walker motifs, and an exofacial large side cavity of yet unknown function. Docking sites were found for the glucose substrate and its inhibitors: glucose, forskolin, and phloretin at the exofacial infundibulum; forskolin, and phloretin at an endofacial site next to the channel opening; and cytochalasin B at a positively charged endofacial pocket 3 Å away from the channel. Thus, 1SUK accounts for practically all biochemical and mutagenesis evidence, and provides clues for the transport process.

INTRODUCTION

The major facilitator superfamily (MFS, TC No. 2.A.1) is a grouping of TM proteins that transport a wide range of solutes such as amino acids, sugars, nucleotides, organic and inorganic anions, metabolites, neurotransmitters, polyols, etc. (Marger and Saier, 1993). This superfamily, which has over a thousand sequenced members, is present from bacteria to eukaryotes, and includes the glucose transporter facilitator family (GLUT/SLC2A, TC No. 2.A.1.1.28; see Pao et al., 1998). GLUT1 was initially cloned and sequenced from HepG2 cells in 1985 (Mueckler et al., 1985). The cDNA encodes a TM protein of 492 residues (calculated molecular weight 54.2 kDa). There is extensive functional and structural and information on Glut1, obtained by mutagenesis studies on accessibility for cysteins, labeling with mercurial reagents, use of inhibitors for substrate influx and efflux, use of labeled metabolites, antibodies, and digestion by proteases (Hruz and Mueckler, 2001). On the basis of this information plus the prediction of TM helical segments, it is theorized that this protein is constituted by 12 TM helices in two 6-helical domain halves separated by the large intercellular loop between H6 and H7. Consistent with this, putative helical regions contain residues that have been identified as crucial for transport function: G75, G76, G79, N288, and A289 (Olsowski et al., 2000); Q161 (Seatter et al., 1998; Mueckler et al., 1994); V165 (Mueckler and Makepeace, 1997); N317, T321, and P387 (Mueckler and Makepeace, 2002); Q282 (Hruz and Mueckler, 1999; Olsowski et al., 2000); I287 (Hruz and Mueckler, 1999); W388 (Kasahara and Kasahara, 1998; Garcia et al., 1992); and W412 (Garcia et al., 1992).

Exploration of the topology is also consistent with the 12-helix scheme. As illustrations, a conserved motif RXGRR is found in both loops 2–3 and 8–9 (residues R89–R93 and R330–R334, respectively; Sato and Mueckler, 1999). The glycosylation site is at N45, as determined by SDS-PAGE and confirmed by mutagenesis (Asano et al., 1991), and labeling with biotin revealed the extracellular location of residue K300 in the putative loop 7–8 (Preston and Baldwin, 1993).

Studies in patients with the glucose transporter-1 deficiency syndrome (see De Vivo et al., 1991) have located eight more residues crucial for transport in both helical and loop regions: S66 and T310 (Klepper et al., 1999); G91 (Klepper et al., 2001); R126 (Pascual et al., 2002; Brockmann et al., 2001; Wang et al., 2000); E247 and K256 (Pascual et al., 2002); and E146 and R333 (Wang et al., 2000). Recently, studies have appeared in which the previously unknown structure of MFS 12 TM helical proteins has been solved by crystallography. An electronic density map for the oxalate transporter OxlT (TC No. 2.A.1.11.1)

Submitted June 18, 2004, and accepted for publication August 9, 2004.

Address reprint requests to Jorge Fischbarg, Dept. of Physiology, College of Physicians & Surgeons, 630 West 168th St., New York, NY 10032. Tel.: 212-305-9092; Fax: 212-305-2461; E-mail: jf20@columbia.edu.

Abbreviations used: OxlT, oxalate transporter; GlpT, glycerol phosphate transporter; LacY, lactose permease; TC, Transporter Commission; CytB, cytochalasin B.

0006-3495/04/11/2990/10 $2.00

doi: 10.1529/biophysj.104.047886

from *Oxalobacter formigens* was solved to 6.5 Å resolution (Hirai et al., 2002), and subsequently the structures of the glycerol 3-phosphate antiporter GlpT from *Escherichia coli* (TC No. 2.A.1.4.3; see Huang et al., 2003) and the lactose permease proton symporter LacY from *E. coli* (TC No. 2.A.1.5.1, see Abramson et al., 2003) were solved at 3.3 Å and 3.5 Å resolution, respectively.

In lieu of missing crystallographic studies, a few models for Glut1 have been previously advanced. Gould and Holman (1993) based theirs on a hypothetic arrangement of two 6-helical TM domains. Subsequently, Zeng et al. (1996) proposed two possible schemes for helical packing using clusters of four transmembrane segments surrounding a central water-accessible channel for the substrate. A model of Glut3 was built on the basis of the crystallographic structure of a mechanosensitive channel of large conductance, plus general insights from aquaporin 1 (Dwyer, 2001), and a model for Glut1 was developed by us based on a prior scheme for LacY helical packing (Zuniga et al., 2001).

In an alignment of the sequences of the three MFS proteins recently crystallized (OxlT, GlpT, and LacY), the homology difference is 77.5%. However, the secondary structures and helical packing are markedly homologous, which indicates that there may be a universal fold for this family. Therefore it seems feasible to model MFS proteins by homology with those already crystallized, and to compare the resulting structure with experimental results such as those on accessibilities, solvent-exposed surface, densities, helicity, energies, and docking with substrates and inhibitors. We have presently done this for GLUT1; the structure obtained accounts for the biochemical and mutagenic evidence, and gives insight on the molecular mechanism of substrate migration, protein flexibility, and binding sites for glucose and the best-known inhibitors, forskolin, phloretin, and cytochalasin B (CytB). Importantly, the eight residues whose mutation leads to pathogenesis are seen to be located in the immediate vicinity of the transport channel, and are in a region of high relative mobility.

MATERIALS AND METHODS

Homology building

We developed two models, Glut1A and Glut1B. Glut1A was done by homology with the crystal structure of GlpT from *E. coli* (PDB No. 1PW4, see Huang et al., 2003); similarly, GLUT1B corresponded to the structure of LacY from *E. coli* (PDB No. 1PV6, see Abramson et al., 2003). The alignments were done with ClustalW (Thompson et al., 1994) and BLOSUM62 (Henikoff and Henikoff, 1992), with gap penalties of 10 for insertion and 0.1 for extension. As constraints, we used residues experimentally determined to be in loops, namely the glycosylation site N45, the conserved motifs of loops 2–3 and loop 8–9 (89/330RXGRR93/334; see Sato and Mueckler, 1999), loop 6–7 residues 213–269, loop 7–8 K300 (Preston and Baldwin, 1993), and loop 11–12 C429. The homology modeling was done with *Nest*, a program inside the JACKAL suite (Xiang and Honig, 2001) and refinement with MODELLER (Sali and Blundell, 1993). For validation we used PROCHECK (Laskowki et al., 1993), WHATCHECK (van Aalten et al., 1996), and molecular docking experiments. For the correct assignments of residues to transmembrane helices 1 and 2 we used evolutionary modeling; we aligned the templates (Swiss-Prot No. P08194) with a homologous human protein obtained searching with PSIBLAST (Altschul et al., 1997), glucose 6-phosphate translocase from *Homo sapiens* (Swiss-Prot No. O43826), with a homology difference of 40.2%.

Molecular dynamics simulations (MDS)

We used the force-field GROMOS43a (van Gunsteren et al., 1996). The protein was placed in a water box (solvation layer of ~7 Å thickness). All runs were at 300 K with a time step of 2 fs. All bonds were constrained using the LINCS (Hess et al., 1997) algorithm for the protein and SETTLE (Miyamoto and Kollman, 1992) for water. We performed runs for 400 ps and for 2 ns. We used Berendsen's scheme for temperature and pressure coupling for both protein and solvent (water). Electrostatic forces were calculated with the particle-mesh Ewald algorithm. Initial energy minimization was done with the steep descent algorithm (1000 steps) followed by conjugate gradient to a maximum force of 0.1 KJ mol^{-1} nm^{-1}. All simulations were performed with the MDS package GROMACS v3.14 (Lindahl et al., 2001; Berendsen et al., 1995). For trajectory analysis we used the tools included in GROMACS and VMD v1.82 (Humphrey et al., 1996); the first 100 ps (equilibration) were neglected.

Transport channel prediction

To determine the passageway and cavities graphically we used VOIDOO (Kleywegt and Jones, 1994) to generate the protein surface with a probe radius of 1.2 Å and grid spacing of 0.5 Å. Subsequently we used MAPMAN (Kleywegt and Jones, 1996) to convert between the *.ezd* and *.mask* formats, and the passageway surface was calculated using the script *cavities.mamac* in the program MAMA (Kleywegt and Jones, 1999). We used VMD (Humphrey et al., 1996) to display graphical images.

Docking

The ligand coordinates for β-D-glucose and forskolin were obtained from the PDBsum database (Laskowski et al., 1997; http://www.biochem.ucl.ac.uk/bsm/pdbsum); phloretin and CytB were built manually and optimized with the MM+ force field in HYPERCHEM. A GROMACS-compatible file for dihedrals and topology was generated for each with the server PRODGR (van Aalten et al., 1996) using the total-charge option, and not minimized. We prepared the initial Glut1A model for docking by running the 400-ps MDS in water referred to above. Docking for each ligand was explored separately using ZDOCK 2.3 (Chen and Weng, 2002) in its default global-scanning mode, so that the program found the docking sites without intervention of the operator. The setting for ''densities'' (angular steps) was 6°, and for clusters of docking results we selected the 100 best. Promising docking results were subject to a further test by solvating with a water layer of ~7 Å and running MDS for 100 ps with particle-mesh Ewald for electrostatic interactions (GROMACS force field). Analysis of binding site results was done with SPDBV 3.7 (Guex and Peitsch, 1997) and the tools from GROMACS (Berendsen et al., 1995; Lindahl et al., 2001).

RESULTS

The model

As explained in Materials and Methods, Glut1 models were obtained by homology with both the *E. coli* glycerol phosphate transporter (Glut1A)and the *E. coli* lac permease structure (Glut1B). Of these two, Glut1B presented substantially more gaps in the helical regions. In addition, a

BLAST search finds no homologies for lac permease in the protein mammalian database. In contrast, there are a few human homologs for the bacterial glycerol phosphate transporter, most notably the glucose-6-phosphate translocase. Hence, we did further analysis only with Glut1A. We used the sequence of glucose-6-phosphate translocase as an intermediate to correct residue assignments for Glut1 (see Materials and Methods), and were thus able to model for all 492 residues of Glut1.

The refined Glut1 model thus obtained by homology with GlpT was subject to extensive validation analysis. Statistical validations for bond lengths and angles and Ramachandran analysis were obtained with PROCHECK, and are shown in Table 1. This program, although permissive, is a first test that a model must definitely meet to be validated. The Glut1 model has no residues in the disallowed region, and has an excellent score (0.3) for the overall *G*-factor (bond lengths and angles). By comparison with our prior (Zuniga et al., 2001) Glut1 model (Table 1), the current model has a larger number of residues in the core. In addition, the prior *G*-factor was deficient for a refined model. This trend continues with the data of Table 2, obtained with WHATCHECK, in which the Ramachandran plot appearance *Z*-score (RPA, col. 3) for Glut1 is exceedingly good (−0.8). In all likelihood, the BBC and IOD parameters appear excessive only because the databases are not optimized for membrane proteins. Still, the Glut1 model scores are similar to those of the crystallographic structures. In several instances in Tables 1 and 2, the scores for Glut1 are better than those for the crystal structures. This is only due to the fact that the crystal structures have not had extensive refinement. Still, the scores also mean that no shortcomings are apparent for the Glut1 structure.

Fig. 1 shows a cartoon representation of the three-dimensional structure of the Glut1 homology model. The helical arrangement shown is the same as what is emerging as a characteristic of the MFS fold, namely, helices 1, 2, 4, 5, 7, 8, 10, and 11 immersed in a box formed by helices 3, 6, 9, and 12. In the view from the top (Fig. 1 *b*), Glut1 dimensions are ~36 × 26 Å, and from the bottom (Fig. 1 *c*), ~46 by 27 Å. Its height is ~61 Å and its shape is trapezoidal (Fig. 1 *a*). The tilts for the different helices vary, as shown in Fig. 1, *b* and *c*. Helix 10 has a small loop in the middle that presumably adds flexibility. The topology is consistent with the experimental constraints from the literature, described in the Introduction. As shown in Fig. 1 *a*, on the extracellular side, the glycosylation site N45 is in loop 1–2, the K300 site corresponds to loop 7–8, and the residue C429 is included in loop 11–12. Intracellularly, loops 2–3 and 7–8 are characterized by the common motif RXGRR. As in its GlpT template, the long loop 6–7 (residues 208–263) presents a short helix between residues R253 and E261.

TABLE 1 Ramachandran plot results and PROCHECK summary

	Ramachandran plot (%)				
Structure	Core	Allowed	Generous	Disallowed	Overall G-factor
Glut1*	86.7	12.4	1.0	0	0.3
GlpT†	85.4	13.5	1.1	0	3.0
LacY‡	79.5	18.6	1.4	0.5	3.4
Glut1§ (old)	81.5	16.9	1.7	0	−3.7

*PDB No. 1SUK.
†PDB No. 1PW4.
‡PDB No. 1PV6.
§PDB No. 1JA5.

TABLE 2 WHATCHECK *Z*-scores for quality assessment and statistical analysis of Glut1, GlpT, and LacY

	Structure *Z*-score						RMS Z-scores			
Structure	PQ	RPA	χNR	BBC	BL	BA	ΩR	SCP	IDD	IOD
Glut1*	−2.0	−0.8	−2.7	−9.5	1.0	1.4	0.9	1.5	1.4	1.3
GlpT†	−2.3	−5.0	−2.2	−8.8	0.7	1.0	0.5	1.1	1.0	1.2
LacY‡	−2.4	−7.9	−4.7	−7.8	0.6	0.8	0.2	0.3	0.6	1.2

PQ, second-generation packing quality; *RPA*, Ramachandran plot appearance; *χNR*, χ^{-1}/χ^{-2} rotamer normality; *BBC*, backbone conformation; *BL*, bond lengths; *BA*, bond angles; Ω, omega angle restraints; *SCP*, side-chain planarity; *IDD*, improper dihedral distribution; and *IOD*, inside/outside distribution.
*PDB No. 1SUK.
†PDB No. 1PW4.
‡PDB No. 1PV6.

Channel and crucial residues

The Glut1 structure is characterized by a channel across the protein that communicates the extracellular and intracellular

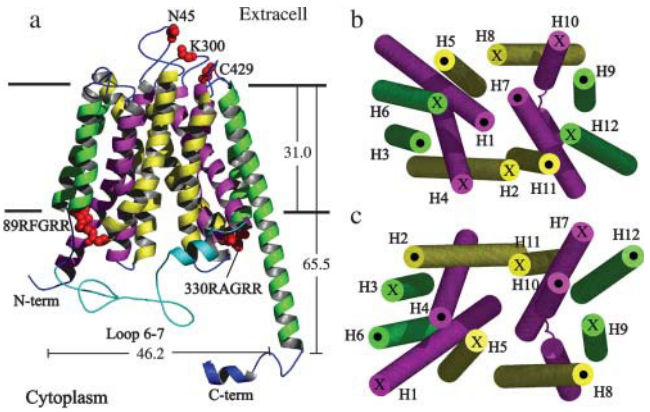

FIGURE 1 Representations of Glut1. (*a*) Side view showing relative positions of the helices. Residues in red represent topology constraints derived from experimental results (explained in the text) involving N45, K300, and C429 for the extracellular side, and motifs 89RFGRR93 and 330RAGRR for the cytoplasmic side. Glut1 measures ~35.6 × 26.3 Å viewed from the top, and 46.2 Å × 27.2 Å from the bottom. Its height is ~61 Å. (*b*) View from the extracellular side showing the tilt of the 12 transmembrane helices. *X* marks loops entering, whereas dots mark loops exiting. (*c*) Cytoplasmic view; marks as above. The helix colors are in concordance with the symmetry template found by Hirai et al. (2002). Figure drawn using PYMOL (http://pymol.sourceforge.net/).

environments. Only one opening is apparent at each one of its ends. The cavities forming the channel and close to it were determined by software (compare to Materials and Methods); Fig. 2 shows views of this channel, as well as residues on it that are crucial for transport function and pathogenicity. Some residues crucial for pathogenicity (Table 3) are found in helices 2 and 4; as can be seen in Fig. 1, these structures limit the transport channel. Other residues crucial for pathogenicity are in the long intracellular loop 6–7, as E247 and K256. Several residues crucial for transport of β-D-glucose bound the channel, most of them located in a channel segment between T310 and the Q161. This segment is ~15 Å long and 7 Å wide. As Fig. 2 shows, another cluster of residues crucial for pathogenicity (G91, E146, E247, K256, and R333) appears bordering the cytoplasmic end segment of the channel. Fig. 3 displays a close-up view of the central segment of the channel, highlighting residues crucial for transport and selectivity.

In addition, we explored interactions between pairs of residues at places where the structure places two helices in close vicinity (3–5 Å). Table 4 lists these pairs. Interactions with helices 3, 6, 9, and 12 were omitted for brevity, as no pathogenic or crucial residues have been located to them yet.

Cavities

Fig. 4 *a* shows ''cavities'' inside the protein, including the channel, as calculated with CASTP. The external cavity appears to be the continuation of the channel, except for a constriction that separates the two (extracellular end of the channel). The two charged cavities are lined with positively charged residues, and correspond to the Walker ATP binding motifs A and B described and analyzed by Liu et al. (2001). After a short (400 ps) molecular dynamics simulation, as shown in Fig. 4 *b*, the extracellular end of the channel widens and a communication opens with the external cavity. At the same time, the intracellular end narrows and a new cavity around the Q161 is segregated from it, the internal cavity; this results in a constriction at that point closing the intracellular end of the channel. Lastly, the intracellular-charged cavity (Walker B ATP binding motif) disappears, as an opening in its place now connects with the main channel. Overall, during the simulation interval the channel increases its volume by the joining of the other cavities to it, but the internal segment of the channel (between the two observed constrictions) is conserved. Areas and volumes of the cavities and the changes that occur after the simulation are shown in Table 5.

TABLE 3 Glut1 pathogenic mutants, resulting in DS-GLUT1 phenotype in humans

Mutation	Nucleotides	Location	Reference
S66F	TCC→TTC	Helix 2	Klepper et al. (1999)
G91D	GGC→GAC	Loop 2–3	Klepper et al. (2001)
R126H	CGC→CAC	Helix 4	Brockmann et al. (2001)
R126L	CGC→CTC	Helix 4	Wang et al. (2000)
R126C	CGC→CGT	Helix 4	Pascual et al. (2002)
E146K	GAA→AAA	Helix 4	Wang et al. (2000)
E247D	GAA→CAA	Loop 6–7	Pascual et al. (2002)
K256V	AAG→GTG	Loop 6–7	Pascual et al. (2002)
T310I	ACC→ATC	Helix 8	Klepper et al. (1999)
R333W	CGG→TGG	Loop 8–9	Wang et al. (2000)

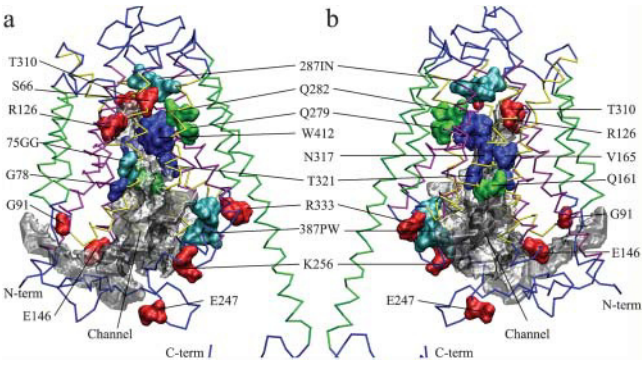

FIGURE 2 Locations of pathologic mutants, residues crucial for activity, and surface calculated for the Glut1 transport pathway. (*a*) The backbone is represented in ribbons and colored as in Fig. 1. Residues are in space-filling mode and labeled; residues crucial for pathogenicity are in red, and those crucial for transport in blue. Cyan denotes a motif of two consecutive residues crucial for transport, and green denotes the Gln residues presumed involved in selectivity. The transport pathway is denoted by a surface representation in gray; it was calculated with the USF programs (http://alpha2.bmc.uu.se/gerard/manuals/welcome2usf.html; Kleywegt and Jones, 1994, 1996, 1999) and read in ccp4 format into the program used for this figure, VMD (http://www.ks.uiuc.edu/Research/vmd/; Humphrey et al., 1996). (*b*) Back view, using the same colors and representations.

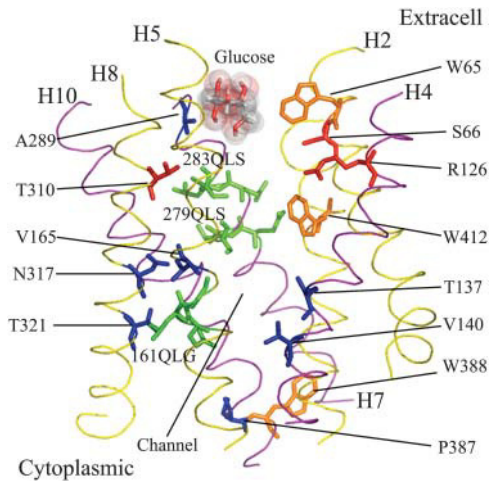

FIGURE 3 Side view to detail the helical ribbons surrounding the putative channel. Helix 1 not shown for clarity. Residues that affect Glut1 function upon mutation are highlighted (side chains shown as sticks). Residue coding: blue, crucial for transport; orange, tryptophans lining the channel (W388 and W412 are crucial for transport); and green, QLS and QLG motifs.

TABLE 4 Helix-helix interactions; pairs of residues separated by 3–5 Å

Helix intersection	Residue pairs
H2–3	87–95
H2–4	122–68, 123–68, 123–71, 123–64, 123–67, **126**–68, **126**–69, **126**–72, 127–71, 127–75, 129–72, 130–72, 130–76, 131–75, 133–72, 134–83, 135–83, 135–87, 139–87, 142–87, 142–88
H2–7	290–65
H2–11	405–77, 409–77, 409–74, *412*–70, *412*–72, *412*–73, *412*–69, 416–**66**, 416–67, 416–70, 420–63, 420–**66**
H4–5	148–151, 152–144, 152–141, 152–145, 155–144, 156–141, 156–144, 159–140, 159–144,
H5–7	289–172
H5–8	306–172, 307–173, 307–176, **310**–169, **310**–173, **310**–172, 311–169, 311–173, 313–169, 314–*165*, 314–169, *317*–*165*, 318–*165*, 318–166, 322–162
H7–8	306–289, 309–*288*
H7–10	369–284, 369–288, 372–284, 373–284, 373–285, 376–277, 376–280, 377–281, 380–277, 381–278, 384–270, 384–274, *387*–270, *388*–270, *388*–267, *388*–271
H7–11	403–271, 403–274, 406–271, 407–274, 407–275, 407–278, 408–278, 410–275, 411–275, 411–278, 411–*279*, *412*–282, 414–*279*, 415–283, 415–*279*, 420–287, *279*–411HB
H8–10	366–308, 366–309, 366–312, 369–309, 369–313, 370–316, 373–*317*, 373–313, 374–320, 375–320, 379–320, 379–324, 365–305HB
H10–11	399–*388*, 400–385, 400–*388*, 400–389, 400–386, 402–*388*, 403–385, 403–*388*, 404–385

Bold, pathogenic residues; italicized, residues crucial for transport. All interactions are hydrophobic except those labeled *HB* (hydrogen bond). Interactions involving helices 1, 3, 6, and 9 omitted (data available upon request).

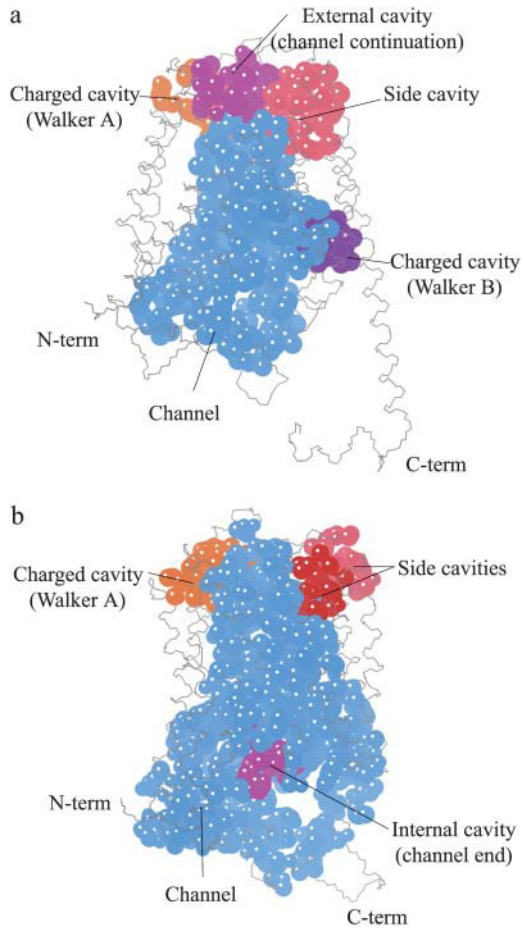

FIGURE 4 Glut1 cavities before and after a 400-ps molecular dynamics simulation. (*a*) Starting conformation. Residues lining the transport pathway are colored in cyan. There are in addition several cavities facing the outside of the protein. The external cavity (*magenta*) is a continuation of the channel, separated from it by an obstruction or neck. There are other cavities, namely, a side cavity (*red*), and two cavities bound by charged residues including ATP binding motifs (Walker A, *orange*; Walker B, *violet*). (*b*) Conformation after 400 ps. The pathway has expanded as the Walker B cavity has fused with it, but an internal cavity (*magenta*) has now appeared at the intracellular end of the channel, separated from it by a neck. The side cavity has divided into two: side cavity 1 (*light red*) and side cavity 2 (*dark red*). Figure drawn using KING (http://kinemage.biochem.duke.edu/software/king.php).

Docking

Fig. 5 shows space-filling displays of putative docking sites for the substrate β-D-glucose (*red*) and several well-known inhibitors of Glut1, forskolin (*green*), phloretin (*magenta*), and CytB (*blue*). Glucose, forskolin, and phloretin dock to what appears to be a common extracellular binding site near the extracellular opening of the transport channel. Interestingly, forskolin and phloretin also dock to an intracellular site near the intracellular opening of the transport channel; this site coincides with the internal cavity that forms after the simulation (Fig. 4 *b*). CytB docks to another site that is located further intracellularly but also along the transport channel described in Fig. 2 *a*. Details of the dockings are given in the sticks representations of Fig. 5, *b*–*g*. Glucose (Fig. 5 *b*) forms two H-bonds and its C6 interacts with Tryptophan 65. At the extracellular site, forskolin (Fig. 5 *c*) forms three H-bonds and again interacts with Trp^{65}, and phloretin (Fig. 5 *d*) also forms three H-bonds, one of them with the aromatic N of Trp^{65}. At its intracellular site, forskolin (Fig. 5 *e*) forms five H-bonds and may interact with Phe^{81}, and phloretin (Fig. 5 *f*) forms six H-bonds, and may interact with Phe^{81}. Lastly, CytB (Fig. 5 *g*) forms only one H-bond, indicating docking by steric hydrophobic interactions. Aside from the sites shown, all ligands except for CytB formed other clusters of interactions with lesser scores, which are not shown. CytB docked at only one site.

DISCUSSION

The results obtained with PROCHECK and WHATCHECK (Tables 1 and 2) provide excellent validation for the Glut1 coordinates given here. The scores for Glut1 are as good as

TABLE 5 Cavity analysis using CASTP

Time	Cavity	Area (nm^2)	Vol (nm^3)	N openings
0	Channel	2785.152	2438.7	3
0	External	190.409	69.3	2
0	Side	169.298	84.7	1
0	Charged ext. (Walker A)	131.336	45.1	2
0	Charged int. (Walker B)	71.386	26.3	0
100	Channel	5372.912	6027.3	15
100	Internal	93.605	58.0	2
100	Charged	164.204	50.2	2
100	Side 1	78.299	22.0	2
100	Side 2	40.645	5.1	0

those for the comparison crystallographic structures. The few scores in Table 2 that exceed the accepted norm are due to insufficient inclusion of transmembrane proteins to arrive at database parameters. A prior Glut1 model of ours, 1JA5 (Zuniga et al., 2001), was based on a helical packing scheme for lac permease that was found inexact when that protein was solved by crystallography (Abramson et al., 2003). We term our prior model obsolete, and instead recommend the use of the current one (1SUK), based on homology with a crystallographic structure. The only qualification is that, as in the GlpT template, 1SUK has a very long helix 12, a result of the mutational engineering done to stabilize the crystals of GlpT. After even a short equilibration (200 ps), helix 12 in 1SUK breaks after Lys^{451}, becoming a C-terminal loop (except for a short local helix).

The structure obtained by homology analysis (and communicated, Salas-Burgos et al., 2004, to the protein database) is the one represented in Figs. 1, 2, and 4 *a*. To examine functional aspects of the transporter, we deemed advisable to remove from the homology structure possible effects of the immobilization required for the crystallographic template, which is why the structure was subject to the short 400-ps simulation described resulting in a ''relaxed'' structure (Fig. 4 *b*). It is well accepted (Carruthers, 1990) that Glut1 has two conformations for glucose binding, one intracellular and other extracellular. From Glut1 turnover rates (120–450/s, Walmsley et al., 1998) a minimum estimate for the time interval required for a conformational change is ~1 ms. Obviously only a small fraction of the entire relevant conformational space can be sampled in 400 ps. Still, the short simulation may yield partial glimpses of the overall conformational change: an internal binding site is formed, and the Walker B motif fuses with the channel. Both Walker motifs have been reported to exert influence on transport through Glut1 (Liu et al., 2001). The presence of

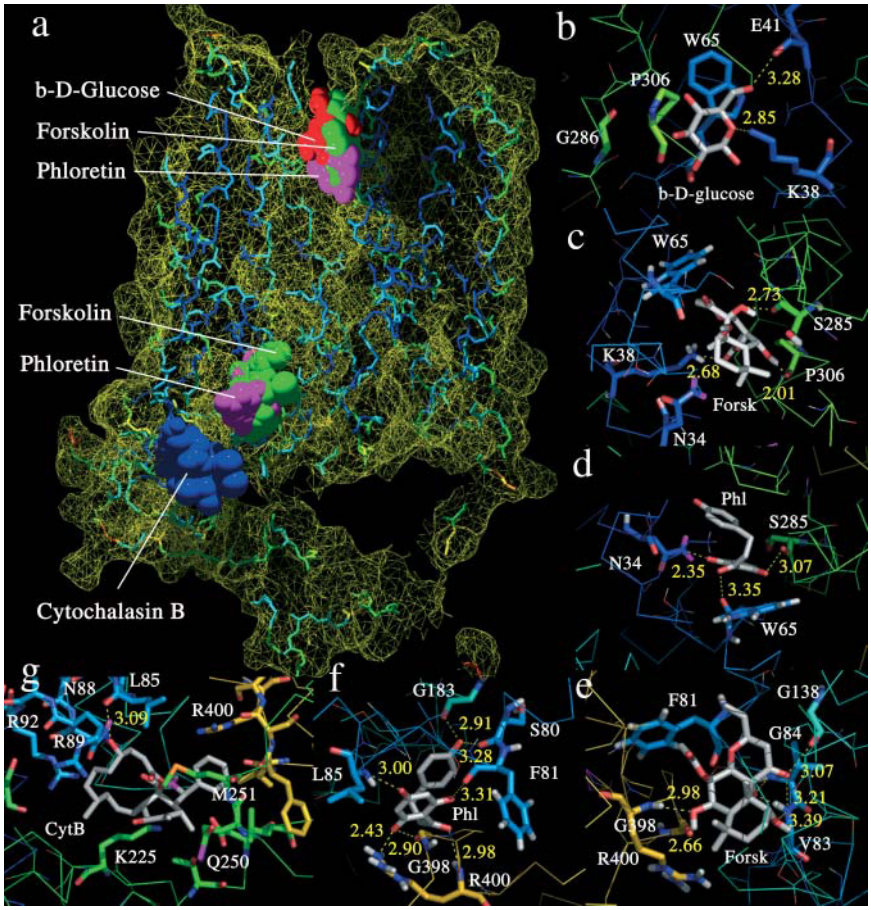

FIGURE 5 Docking sites for substrates and characteristic inhibitors of Glut1. (*a*) Substrates and inhibitors at their docking sites. Slab view showing the cavities and transport pathway of Glut1. β-D-glucose (*red*) binds extracellularly, whereas both forskolin (*green*), and phloretin (*magenta*) bind at extracellular and intracellular sites. Cytochalasin B (*blue*) binds intracellularly. Figure drawn using SPDBV (http://us.expasy.org/spdbv/; Guex and Peitsch, 1997). Docking sites for (*b*), glucose; (*c*) forskolin (extracellular); (*d*) phloretin (extracellular); (*e*) forskolin (intracellular); (*f*) phloretin (intracellular); and (*g*), cytochalasin B. White labels, residues; yellow sticks, hydrogen bonds. Numbers indicate Å distances.

charged cavities in our model therefore provides a possible framework for observed modulation of transport by ATP (Carruthers and Helgerson, 1989; Liu et al., 2001; Cloherty et al., 2001).

The central channel is essentially formed by helices 2, 4, 5, 7, 8, and 10. The residues crucial for transport and pathogenicity (Fig. 2) are nucleated in two groups: one around the central channel, and the other on the long intracellular loop. The functional consequences observed are quite consistent with the model. The presence of solvent-accessible residues along the transport channel (Fig. 2) is logical in this context. In addition, a line of residues crucial for pathogenicity (E247, K256, R333) or transport (P387, W388) is located (Fig. 2) on or near the segment of the long intracellular loop that delimits the transport pathway, which again lends credence to the model.

We also explored the hydrophobic interactions between pairs of residues at points where helices cross each other. We hypothesized that mutations at those residues could affect packing or stability, with consequent effects on function. Table 4 shows these residues; as can be seen, mutations of some of them have been already determined to result in pathogenicity or to affect transport. It may be useful to study what effects could result from mutations at the other sites identified here, hitherto unexplored.

The shape of the transport pathway is noteworthy. The entrance at the extracellular end is funnel-like (*infundibulum*, Fig. 4 *a*), and at its bottom we find the docking sites described below. As for the intracellular end, interestingly, the horn-shaped pathway incurvates so that its exit is located almost to the side of the protein. It also expands into a cylindrical cavity ~12 Å in diameter. Fittingly, prior observations from Carruthers' laboratory (Heard et al., 2000; Cloherty et al., 2002) of a delay in the substrate exiting the protein during influx had been already interpreted in terms of a cytoplasmic cavity in Glut1 (Heard et al., 2000; Cloherty et al., 2002). In addition, the position of the cytoplasmic orifice near the side of the protein would allow both monomer cytoplasmic cavities to join into a larger one for a dimer, as also predicted by Carruthers and co-workers (Heard et al., 2000; Cloherty et al., 2002).

Glucose (β-D-glucopyranose) is at the same time hydrophilic due to its OH groups, and hydrophobic due to the pyranose ring. In *E. coli* maltoporin, a ''greasy slide'' made of aromatic residues has been linked to sugar transport (Van Gelder et al., 2002). Interestingly, in our model the internal segment of the transport pathway (the channel) is lined by both hydrophilic and hydrophobic residues. Among them, many have been mutated and shown to be crucial for transport activity—Q161, R126, Q279, Q282, N317, T321, W65, W388, W412, and V165 (all cited above). These characteristics are shown in detail in Fig. 3.

The conserved QLS motif starting at Q279 has been recognized as crucial for the selectivity of Gluts for the transported sugars (Seatter et al., 1998; Olsowski et al., 2000). Fittingly, it is near the extracellular entrance of the channel (Fig. 3), possibly positioned to discriminate against nonsubstrates attempting to enter the cell. Moreover, the sequence at that point is (279)QLSQQLS. As pointed out recently (Li et al., 2004), at the second QLS site (one helix turn up from the first, at Q283), except for Glut11, the QQLS motif is very well conserved in all Gluts (1–14). This site is at the very extracellular end of the channel (Fig. 3), which forms a bottleneck there (Fig. 4 *b*). It is easy to speculate that this site may be also involved in selectivity, perhaps somehow interacting with the QLS site down the helix. Lastly, there is a QLG motif starting at position 161 (Fig. 3). Mueckler et al. (1994) established that mutations of the well-conserved Q161 residue decreased transport 10–50-fold. In our model, this QLG motif is at the intracellular end of the channel; if by analogy with the QLS this motif can also select substrates, it would be positioned to select molecules exiting the cell.

Even if speculative, there is a mechanism for substrate migration consistent with the model. It seems unlikely that glucose would form more than one or temporarily two H-bonds at any time. Formation of more H-bonds would stabilize the substrate in position, keeping it in place rather than facilitating migration. However, if glucose forms approximately one H-bond at a time, it could migrate along the channel by rolling along the wall, forming a new H-bond forward as the one in the back is being broken. Such rolling and sequential H-bonding has been seen by us in molecular dynamics simulations (unpublished data); H-bonding of the glucose substrate with crucial residues was seen in a molecular dynamics simulation done with a Glut3 model (Dwyer, 2001). Moreover, the role of the hydrophobic residues would be to develop a stabilizing interaction with the hydrophobic C6 region of the substrate as it passes by. Such an interaction is seen in the glucose docking site shown in Fig. 5, *a* and *b*.

Docking sites

As can be seen in Fig. 5, glucose, forskolin, and phloretin dock at sites in very close mutual proximity on the exofacial vestibule of the Glut1 model; the model is consistent with great steric interference by the inhibitors with the exofacial glucose docking site. Regarding forskolin and glucose, in an analysis of interactions of both with Glut1 it was concluded that a carbohydrate was recognized within the forskolin functionalities (Joost et al., 1988). As for phloretin, its phenol ring appears to sit in the same pocket as glucose, and is stabilized in place by three H-bonds to its benzene-1,3,5-triol ring. As one would expect, the inhibitors develop more interactions than glucose with the protein (Fig. 5), which would of course stabilize them in place so as to obstruct glucose docking.

The interactions of forskolin with its exofacial site resemble those of glucose (compare to K38, W65, Fig. 5, *b* and *c*). We speculate therefore that there may be a potential

docking site for glucose at or near the forskolin endofacial site, but it is not made evident in the particular conformation sampled by the simulation. If that would be the case, one would predict competitive inhibition of glucose transport by both forskolin and phloretin at both exofacial and endofacial sites. There are findings in the kinetic literature that are consistent with two binding sites (Helgerson and Carruthers, 1987) and the inherent complex behavior (Carruthers, 1990). Interestingly, anomalous kinetics in Glut1 have also been accounted for in a kinetic scheme (Hernandez et al., 1996) with two sites and two conformational states.

As mentioned above, the putative recognition site for sugars, the QLS motif, is at the extracellular end of the channel, and there is a QLG site at the intracellular end of the channel. The docking algorithm does not find glucose at those sites. It is conceivable that this may be due to the particular channel conformation sampled in the simulation. However, gossypol, which has been linked to inhibition of glucose transport (Christensen et al., 1987), is found at sites inside the channel by the docking algorithm (data not shown). From this we presume that if glucose would bind strongly inside the channel, the docking algorithm would find it there; it does not. This seems logical; as the substrate enters the channel, it would be most efficient if it would traverse it quickly. In this context, selectivity sites inside the channel would allow passage or not, but would not bind substrate tightly.

Concerning another well-known Glut1 inhibitor, CytB, the docking algorithm found for it only one cluster with very high score, and no other clusters at all. It was on the intracellular side, as experiments had shown (Helgerson and Carruthers, 1987; Carruthers, 1990). However, the site (Fig. 5 *g*) is different than that predicted by several other studies (with interactions with helices 10 and 11; Baldwin, 1993) near W388 (Garcia et al., 1992; Kasahara and Kasahara, 1998). Still, the present findings are internally consistent in that the CytB site is close (3 Å) to the endofacial site for forskolin and phloretin (Fig. 5, *a* and *e–f*), and close enough to the endofacial channel opening to interfere with glucose passage. It seems noteworthy that the present CytB site appears to be a pocket lined with several positively charged and polar residues (Fig. 5 *g*), which might attract a molecule with moderate dipole moment such as CytB.

The role of the cavities described here is unclear. On the other hand, there is a body of literature on compounds that interact with Glut1 and may exert regulatory influence on it, namely nucleotides and analogs, flavonoids, antiestrogens, androgens, antiandrogens, barbiturates, and catechins (Honkanen et al., 1995; Afzal et al., 2002; Martin et al., 2003; Naftalin et al., 2003). Perhaps the cavities may act as binding sites for such modulators.

In summary, there is ample evidence to validate the present model of Glut1. It arises from a crystallographic structure template, it stands optimally in terms of statistics and energetics, and accounts for practically all published biochemical, physiological, and mutagenesis evidence. Some aspects that remain to be elucidated include the binding site for CyB and the existence and location of an endofacial binding site(s) for glucose. Still, the present model may be useful in elucidating the connection between the structure and the function of Glut1 and related molecules.

The present Glut1 coordinates have been communicated to the RCSB Protein Data Bank (entry No. 1SUK).

This work was supported by National Institutes of Health grant EY08918 (to J.F.), and in part by Research to Prevent Blindness grant 1020451 from FONDECYT, Chile, and grant DIUC-201034.0061.4 from the University of Concepción. Felipe Zúñiga is a predoctoral fellow from CONICYT, Chile.

REFERENCES

Abramson, J., I. Smirnova, V. Kasho, G. Verner, H. R. Kaback, and S. Iwata. 2003. Structure and mechanism of the lactose permease of *Escherichia coli*. *Science*. 301:610–615.

Afzal, I., P. Cunningham, and R. J. Naftalin. 2002. Interactions of ATP, oestradiol, genistein and the anti-oestrogens, faslodex (ICI 182780) and tamoxifen, with the human erythrocyte glucose transporter, GLUT1. *Biochem. J.* 365:707–719.

Altschul, S., T. Madden, A. Schaffer, J. Zhang, Z. Zhang, W. Miller, and D. Lipman. 1997. Gapped BLAST and PSI-BLAST: a new generation of protein database search programs. *Nucleic Acids Res.* 25:3389–3402.

Asano, T., H. Katagiri, K. Takata, J. L. Lin, H. Ishihara, K. Inukai, K. Tsukuda, M. Kikuchi, H. Hirano, and Y. Yazaki. 1991. The role of *n*-glycosylation of GLUT1 for glucose transport activity. *J. Biol. Chem.* 266:24632–24636.

Baldwin, S. A. 1993. Mammalian passive glucose transporters: members of an ubiquitous family of active and passive transport proteins. *Biochim. Biophys. Acta*. 1154:17–49.

Berendsen, H. J. C., D. van der Spoel, and R. van Drunen. 1995. GROMACS: a message-passing parallel molecular dynamics implementation. *Comp. Phys. Comm.* 91:43–56.

Brockmann, K., D. Wang, C. G. Korenke, A. von Moers, Y. Y. Ho, J. M. Pascual, K. Kuang, H. Yang, L. Ma, P. Kranz-Eble, J. Fischbarg, F. Hanefeld, and D. C. De Vivo. 2001. Autosomal dominant Glut-1 deficiency syndrome and familial epilepsy. *Ann. Neurol.* 50:476–485.

Carruthers, A. 1990. Facilitated diffusion of glucose. *Physiol. Rev.* 70:1135–1175.

Carruthers, A., and A. L. Helgerson. 1989. The human erythrocyte sugar transporter is also a nucleotide binding protein. *Biochemistry*. 28:8337–8346.

Chen, R., and Z. Weng. 2002. Docking unbound proteins using shape complementarity, desolvation, and electrostatics. *Proteins*. 47:281–294.

Christensen, R. L., D. L. Shade, C. B. Graves, and J. M. McDonald. 1987. Evidence that protein kinase C is involved in regulating glucose transport in the adipocyte. *Int. J. Biochem.* 19:259–265.

Cloherty, E. K., S. Hamill, K. Levine, and A. Carruthers. 2001. Sugar transporter regulation by ATP and quaternary structure. *Blood Cells Mol. Dis.* 27:102–107.

Cloherty, E. K., K. B. Levine, C. Graybill, and A. Carruthers. 2002. Cooperative nucleotide binding to the human erythrocyte sugar transporter. *Biochemistry*. 41:12639–12651.

De Vivo, D. C., R. R. Trifiletti, R. I. Jacobson, G. M. Ronen, R. A. Behmand, and S. I. Harik. 1991. Defective glucose transport across the blood-brain barrier as a cause of persistent hypoglycorrhachia, seizures, and developmental delay. *N. Engl. J. Med.* 325:703–709.

Dwyer, D. S. 2001. Model of the 3-D structure of the GLUT3 glucose transporter and molecular dynamics simulation of glucose transport. *Proteins*. 42:531–541.

Garcia, J. C., M. Strube, K. Leingang, K. Keller, and M. M. Mueckler. 1992. Amino acid substitutions at tryptophan 388 and tryptophan 412 of the HepG2 (Glut1) glucose transporter inhibit transport activity and targeting to the plasma membrane in *Xenopus* oocytes. *J. Biol. Chem.* 267:7770–7776.

Gould, G. W., and G. D. Holman. 1993. The glucose transporter family: structure, function and tissue-specific expression. *Biochem. J.* 295:329–341.

Guex, N., and M. C. Peitsch. 1997. SWISS-MODEL and the Swiss-PDB Viewer: an environment for comparative protein modeling. *Electrophoresis*. 18:2714–2723.

Heard, K. S., N. Fidyk, and A. Carruthers. 2000. ATP-dependent substrate occlusion by the human erythrocyte sugar transporter. *Biochemistry*. 39:3005–3014.

Helgerson, A. L., and A. Carruthers. 1987. Equilibrium ligand binding to the human erythrocyte sugar transporter. Evidence for two sugar-binding sites per carrier. *J. Biol. Chem.* 262:5464–5475.

Henikoff, S., and J. G. Henikoff. 1992. Amino acid substitution matrices from protein blocks. *Proc. Natl. Acad. Sci. USA*. 89:10915–10919.

Hernandez, J. A., J. Fischbarg, and J. C. Vera. 1996. Modeling facilitative sugar transporters: transitions between single and double ligand occupancy of multiconformational channel models explain anomalous kinetics. *J. Membr. Biol.* 149:57–69.

Hess, B., H. Bekker, H. J. C. Berendsen, and J. G. E. M. Fraaije. 1997. LINCS: a linear constraint solver for molecular simulations. *J. Comput. Chem.* 18:1463–1472.

Hirai, T., J. A. Heymann, D. Shi, R. Sarker, P. C. Maloney, and S. Subramaniam. 2002. Three-dimensional structure of a bacterial oxalate transporter. *Nat. Struct. Biol.* 9:597–600.

Honkanen, R. A., H. McBath, C. Kushmerick, G. E. Callender, S. F. Scarlata, J. D. Fenstermacher, and H. C. Haspel. 1995. Barbiturates inhibit hexose transport in cultured mammalian cells and human erythrocytes and interact directly with purified GLUT-1. *Biochemistry*. 34:535–544.

Hruz, P. W., and M. M. Mueckler. 1999. Cysteine-scanning mutagenesis of transmembrane segment 7 of the GLUT1 glucose transporter. *J. Biol. Chem.* 274:36176–36180.

Hruz, P. W., and M. M. Mueckler. 2001. Structural analysis of the GLUT1 facilitative glucose transporter. *Mol. Membr. Biol.* 18:183–193. (Review.)

Huang, Y., M. J. Lemieux, J. Song, M. Auer, and D. N. Wang. 2003. Structure and mechanism of the glycerol-3-phosphate transporter from *Escherichia coli*. *Science*. 301:616–620.

Humphrey, W., A. Dalke, and K. Schulten. 1996. VMD: visual molecular dynamics. *J. Mol. Graph.* 14:33–38.

Joost, H. G., A. D. Habberfield, I. A. Simpson, A. Laurenza, and K. B. Seamon. 1988. Activation of adenylate cyclase and inhibition of glucose transport in rat adipocytes by forskolin analogues: structural determinants for distinct sites of action. *Mol. Pharmacol.* 33:449–453.

Kasahara, T., and M. Kasahara. 1998. Tryptophan 388 in putative transmembrane segment 10 of the rat glucose transporter Glut1 is essential for glucose transport. *J. Biol. Chem.* 273:29113–29117.

Klepper, J., I. Monden, E. Guertsen, T. Voit, M. Willemsen, and K. Keller. 2001. Functional consequences of the autosomal dominant G272A mutation in the human GLUT1 gene. *FEBS Lett.* 498:104–109.

Klepper, J., D. Wang, J. Fischbarg, J. C. Vera, I. T. Jarjour, K. R. O'Driscoll, and D. C. De Vivo. 1999. Defective glucose transport across brain tissue barriers: a newly recognized neurological syndrome. *Neurochem. Res.* 24:587–594.

Kleywegt, G. J., and T. A. Jones. 1994. Detection, delineation, measurement and display of cavities in macromolecular structures. *Acta Crystallogr.* D50:178–185.

Kleywegt, G. J., and T. A. Jones. 1996. xdlMAPMAN and xdlDATAMAN—programs for reformatting, analysis and manipulation of biomacromolecular electron-density maps and reflection data sets. *Acta Crystallogr.* D52:826–828.

Kleywegt, G. J., and T. A. Jones. 1999. Software for handling macromolecular envelopes. *Acta Crystallogr.* D55:941–944.

Laskowki, R. A., M. W. MacArthur, D. S. Moss, and J. M. Thornton. 1993. PROCHECK: a program to check the stereochemical quality of protein structures. *J. Appl. Crystallog.* 26:283–291.

Laskowski, R. A., E. G. Hutchinson, A. D. Michie, A. C. Wallace, M. L. Jones, and J. M. Thornton. 1997. PDBsum: a Web-based database of summaries and analyses of all PDB structures. *Trends Biochem. Sci.* 22:488–490.

Li, Q., A. Manolescu, M. Ritzel, S. Yao, M. Slugoski, J. D. Young, X. Z. Chen, and C. I. Cheeseman. 2004. Cloning and functional characterization of the human GLUT7 isoform SLC2A7 from the small intestine. *Am. J. Physiol.* 287:G236–G242.

Lindahl, E., B. Hess, and D. van der Spoel. 2001. GROMACS 3.0: a package for molecular simulation and trajectory analysis. *J. Mol. Mod.* 7:306–317.

Liu, Q., J. C. Vera, H. Peng, and D. W. Golde. 2001. The predicted ATP-binding domains in the hexose transporter GLUT1 critically affect transporter activity. *Biochemistry*. 40:7874–7881.

Marger, M. D., and M. H. Saier, Jr. 1993. A major superfamily of transmembrane facilitators that catalyse uniport, symport and antiport. *Trends Biochem. Sci.* 18:13–20.

Martin, H. J., F. Kornmann, and G. F. Fuhrmann. 2003. The inhibitory effects of flavonoids and antiestrogens on the Glut1 glucose transporter in human erythrocytes. *Chem. Biol. Interact.* 146:225–235.

Miyamoto, S., and P. A. Kollman. 1992. SETTLE: an analytical version of the SHAKE and RATTLE algorithms for rigid water models. *J. Comput. Chem.* 13:952–962.

Mueckler, M., C. Caruso, S. A. Baldwin, M. Panico, I. Blench, H. R. Morris, W. J. Allard, G. E. Lienhard, and H. F. Lodish. 1985. Sequence and structure of a human glucose transporter. *Science*. 229:941–945.

Mueckler, M., and C. Makepeace. 1997. Identification of an amino acid residue that lies between the exofacial vestibule and exofacial substrate-binding site of the Glut1 sugar permeation pathway. *J. Biol. Chem.* 272: 30141–30146.

Mueckler, M., and C. Makepeace. 2002. Analysis of transmembrane segment 10 of the Glut1 glucose transporter by cysteine-scanning mutagenesis and substituted cysteine accessibility. *J. Biol. Chem.* 277: 3498–3503.

Mueckler, M., W. Weng, and M. Kruse. 1994. Glutamine 161 of Glut1 glucose transporter is critical for transport activity and exofacial ligand binding. *J. Biol. Chem.* 269:20533–20538.

Naftalin, R. J., I. Afzal, P. Cunningham, M. Halai, C. Ross, N. Salleh, and S. R. Milligan. 2003. Interactions of androgens, green tea catechins and the antiandrogen flutamide with the external glucose-binding site of the human erythrocyte glucose transporter GLUT1. *Br. J. Pharmacol.* 140:487–499.

Olsowski, A., I. Monden, G. Krause, and K. Keller. 2000. Cysteine scanning mutagenesis of helices 2 and 7 in GLUT1 identifies an exofacial cleft in both transmembrane segments. *Biochemistry*. 39:2469–2474.

Pao, S. S., I. T. Paulsen, and M. H. Saier. 1998. Major facilitator superfamily. *Microbiol. Mol. Biol. Rev.* 62:1–34.

Pascual, J. M., R. L. Van Heertum, D. Wang, K. Engelstad, and D. C. De Vivo. 2002. Imaging the metabolic footprint of Glut1 deficiency on the brain. *Ann. Neurol.* 52:458–464.

Preston, R. A., and S. A. Baldwin. 1993. GLUT 1: identification of exofacial lysine-residues. *Biochem. Soc. Trans.* 21:309–312.

Sali, A., and T. L. Blundell. 1993. Comparative protein modelling by satisfaction of spatial restraints. *J. Mol. Biol.* 234:779–815.

Sato, M., and M. Mueckler. 1999. A conserved amino acid motif (R-X-G-R-R) in the Glut1 glucose transporter is an important determinant of membrane topology. *J. Biol. Chem.* 274:24721–24725.

Seatter, M. J., S. A. De la Rue, L. M. Porter, and G. W. Gould. 1998. QLS motif in transmembrane helix VII of the glucose transporter family interacts with the C-1 position of D-glucose and is involved in substrate selection at the exofacial binding site. *Biochemistry.* 37:1322–1326.

Thompson, J. D., D. G. Higgins, and T. J. Gibson. 1994. CLUSTAL W: improving the sensitivity of progressive multiple sequence alignment through sequence weighting, position-specific gap penalties and weight matrix choice. *Nucleic Acids Res.* 22:4673–4680.

van Aalten, D. M., R. Bywater, J. B. Findlay, M. Hendlich, R. W. Hooft, and G. Vriend. 1996. PRODRG, a program for generating molecular topologies and unique molecular descriptors from coordinates of small molecules. *J. Comput. Aided Mol. Des.* 10:255–262.

Van Gelder, P., F. Dumas, I. Bartoldus, N. Saint, A. Prilipov, M. Winterhalter, Y. Wang, A. Philippsen, J. P. Rosenbusch, and T. Schirmer. 2002. Sugar transport through maltoporin of *Escherichia coli*: role of the greasy slide. *J. Bacteriol.* 184:2994–2999.

van Gunsteren, W. F., P. Kruger, S. R. Billeter, A. E. Mark, A. A. Eising, W. R. P. Scott, P. H. Huneberger, and I. G. Tironi. 1996. Biomolecular Simulation: The GROMOS96 Manual and User Guide. BiomosrHochschulverlag AG an der ETH Zurich, Switzerland.

Walmsley, A. R., M. P. Barrett, F. Bringaud, and G. W. Gould. 1998. Sugar transporters from bacteria, parasites and mammals: structure-activity relationships. *Trends Biochem. Sci.* 23:476–481.

Wang, D., P. Kranz-Eble, and D. C. De Vivo. 2000. Mutational analysis of GLUT1 (SLC2A1) in Glut-1 deficiency syndrome. *Hum. Mutat.* 16:224–231.

Xiang, Z., and B. Honig. 2001. Extending the accuracy limits of prediction for side-chain conformations. *J. Mol. Biol.* 311:421–430.

Zeng, H., R. Parthasarathy, A. L. Rampal, and C. Y. Jung. 1996. Proposed structure of putative glucose channel in GLUT1 facilitative glucose transporter. *Biophys. J.* 70:14–21.

Zuniga, F. A., G. Shi, J. F. Haller, A. Rubashkin, D. R. Flynn, P. Iserovich, and J. Fischbarg. 2001. A three-dimensional model of the human facilitative glucose transporter Glut1. *J. Biol. Chem.* 276: 44970–44975.